Nonspherical and Spherical Characterization of Ice in Hurricane Erin for Wideband Passive Microwave Comparisons

Gail Skofronick-Jackson[1], Eric Holthaus[2], Cerese Albers[3], and Min-Jeong Kim[4]

1. NASA Goddard Space Flight Center, Greenbelt, MD
2. Columbia University, New York City, NY
3. Florida State University, Tallahassee, FL
4. NOAA, Camp Springs, MD

Submitted to Journal of Geophysical Research April 10, 2007

Corresponding Author: Gail Skofronick Jackson, Code 614.6, Building 33, Room A428, Greenbelt, MD 20771, 301-614-5720, FAX 301-614-5558, Gail.S.Jackson@nasa.gov

Popular Summary:

In order to better understand the characteristics of frozen cloud particles in hurricane systems, computed brightness temperatures were compared with radiometric observations of Hurricane Erin (2001) from the NASA ER-2 aircraft. The focus was on the frozen particle microphysics and the high frequencies (≥ 85 GHz) that are particularly sensitive to frozen particles. Frozen particles in hurricanes are an indicator of increasing hurricane intensity. In fact "hot towers" associated with increasing hurricane intensity are composed of frozen ice cloud particles. (They are called hot towers because their column of air is warmer than the surrounding air temperature, but above about 5-7 km to the tops of the towers at 15-19 km, the cloud particles are frozen.) This work showed that indeed, one can model information about cloud ice particle characteristics and indicated that non-spherical ice shapes, instead of spherical particles, provided the best match to the observations. Overall, this work shows that while non-spherical particles show promise, selecting and modeling a proper ice particle parameterization can be difficult and additional in situ measurements are needed to define and validate appropriate parameterizations. This work is important for developing Global Precipitation Measurement (GPM) mission satellite algorithms for the retrieval of ice characteristics both above the melting layer, as in Hurricane Erin, and for ice particles that reach the surface as falling snow.

Nonspherical and Spherical Characterization of Ice in Hurricane Erin for Wideband Passive Microwave Comparisons

Gail Skofronick-Jackson[1], Eric Holthaus[2], Cerese Albers[3], and Min-Jeong Kim[4]

1. NASA Goddard Space Flight Center, Greenbelt, MD
2. Columbia University, New York City, NY
3. Florida State University, Tallahassee, FL
4. NOAA, Camp Springs, MD

Submitted to Journal of Geophysical Research April 10, 2007

Corresponding Author: Gail Skofronick Jackson, Code 614.6, Building 33, Room A428, Greenbelt, MD 20771, 301-614-5720, FAX 301-614-5558, Gail.S.Jackson@nasa.gov

Significant Findings:

In order to better understand the characteristics and physical-to-radiative relationships of frozen hydrometeors in hurricane systems, computed brightness temperatures (T_B) from 10.7 to 183±10 GHz were compared with radiometric observations of Hurricane Erin (2001) from the NASA ER-2 aircraft. The focus was on the frozen particle microphysics and the high frequencies (≥ 85 GHz) that are particularly sensitive to frozen particles. There were four significant findings. The first finding was that the MM5 cloud model did not have enough vertical resolution at its highest altitudes to produce the temperature profiles needed to compute T_B in the 55 to 60 GHz range and hence coincident dropsonde data was required. The second significant finding was the ocean surface conditions were difficult to ascertain in the hurricane eye so that brightness temperatures that depended on the surface conditions did not match the observations well. The third finding revealed the importance of the bulk asymmetry parameter (that describes the direction of scattering) in the resultant T_B values. Typically, passive remote sensing has attributed T_B values to the combination of the bulk absorption and scattering parameters, essentially ignoring the role of the asymmetry. The fourth and most important finding was that non-spherical particles, in this case modeled as bullet rosettes, provided the absorption, scattering, and asymmetry radiative properties that when used in the radiative transfer calculations gave the best match to the observations. Overall, this work shows that while non-spherical particles show promise, selecting and modeling a proper ice particle parameterization can be difficult and additional in situ measurements are needed to define and validate appropriate parameterizations. This work is important for developing Global Precipitation Measurement (GPM) mission satellite algorithms for the retrieval of ice characteristics both above the melting layer, as in Hurricane Erin, and for ice particles that reach the surface as falling snow.

Nonspherical and Spherical Characterization of Ice in Hurricane Erin for Wideband Passive Microwave Comparisons

Gail Skofronick-Jackson[1], Eric Holthaus[2], Cerese Albers[3], and Min-Jeong Kim[4]

1. NASA Goddard Space Flight Center, Greenbelt, MD
2. Columbia University, New York City, NY
3. Florida State University, Tallahassee, FL
4. NOAA, Camp Springs, MD

Submitted to Journal of Geophysical Research April 10, 2007

Corresponding Author: Gail Skofronick Jackson, Code 614.6, Building 33, Room A428, Greenbelt, MD 20771, 301-614-5720, FAX 301-614-5558, Gail.S.Jackson@nasa.gov

ABSTRACT:

In order to better understand the characteristics and physical-to-radiative relationships of frozen hydrometeors in hurricane systems, computed brightness temperatures (T_B) from 10.7 to 183±10 GHz were compared with radiometric observations of Hurricane Erin (2001) from the NASA ER-2 aircraft. The focus here is on the frozen particle microphysics and the high frequencies (≥ 85 GHz) that are particularly sensitive to frozen particles. In order to initialize the cloud profiles used in the radiative transfer calculations, data from airborne radars, dropsondes, and cloud models were used. Three different ice parameterizations were used with these cloud profiles to obtain the particle radiative signatures: (1) a solid ice sphere, (2) a low ice density (fluffy) sphere, and (3) a non-spherical bullet rosette habit where the radiation attributes (scattering, absorption, and asymmetry properties) are computed using the Discrete Dipole Approximation. All low frequency calculations track the observations well except in the eye of Hurricane Erin where the surface wind speed and/or near surface temperatures were difficult to model. For the higher frequencies, the solid ice spheres produced T_Bs that were too cold in most cases while the fluffy snow particle parameterizations produced T_Bs that were much warmer than the observations. The comparisons between the calculated and observed T_Bs show that in general the three dimensional rosette habit does the best job of matching the observations for most of the high frequencies because of its scattering and asymmetry parameters. Overall, this work shows that while non-spherical particles show promise, selecting and modeling a proper ice particle parameterization can be difficult and additional in situ measurements are needed to define and validate appropriate parameterizations.

Nonspherical and Spherical Characterization of Ice in Hurricane Erin for Wideband Passive Microwave Comparisons

Gail Skofronick-Jackson[1], Eric Holthaus[2], Cerese Albers[3], and Min-Jeong Kim[4]

1. NASA Goddard Space Flight Center, Greenbelt, MD
2. Columbia University, New York City, NY
3. Florida State University, Tallahassee, FL
4. NOAA, Camp Springs, MD

To be submitted to Journal of Geophysical Research

Submitted: April 12, 2007

Corresponding Author: Gail Skofronick Jackson, Code 614.6, Building 33, Room A428, Greenbelt, MD 20771, 301-614-5720, FAX 301-614-5558, Gail.S.Jackson@nasa.gov

ABSTRACT:

In order to better understand the characteristics and physical-to-radiative relationships of frozen hydrometeors in hurricane systems, computed brightness temperatures (T_B) from 10.7 to 183±10 GHz were compared with radiometric observations of Hurricane Erin (2001) from the NASA ER-2 aircraft. The focus here is on the frozen particle microphysics and the high frequencies (≥ 85 GHz) that are particularly sensitive to frozen particles. In order to initialize the cloud profiles used in the radiative transfer calculations, data from airborne radars, dropsondes, and cloud models were used. Three different ice parameterizations were used with these cloud profiles to obtain the particle radiative signatures: (1) a solid ice sphere, (2) a low ice density (fluffy) sphere, and (3) a non-spherical bullet rosette habit where the radiation attributes (scattering, absorption, and asymmetry properties) are computed using the Discrete Dipole Approximation. All low frequency calculations match the observations reasonably well. For the higher frequencies, the solid ice spheres produced T_Bs that were too cold in most cases while the fluffy snow particle parameterizations produced T_Bs that were much warmer than the observations. The comparisons between the calculated and observed T_Bs show that in general the three dimensional rosette habit does the best job of matching the observations for most of the high frequencies primarily because of its asymmetry coefficients. Overall, this work shows that while non-spherical particles show promise, selecting and modeling a proper ice particle parameterization can be difficult and additional in situ measurements are needed to define and validate appropriate parameterizations.

1. Introduction

The development and strength of tropical cyclones is highly influenced by ice particles in hurricane rain bands and convection [e.g., *McFarquhar et al*, 2006; *Heymsfield et al*, 2006; *Willoughby*, 1998]. In fact "hot towers" associated with increasing hurricane intensity are composed of frozen ice cloud particles. (They are called hot towers because their column of air is slightly warmer than the surrounding air temperature, but above about 5-7 km to the tops of the towers at 15-19 km, the cloud particles are frozen.) However, little information is known about frozen droplet characteristics in hurricane clouds. While cloud resolving models do incorporate frozen particles [e.g., *Wu et al.*, 2006; *Tao et al.*, 2007], in general these modeled particles are only validated with extremely sparse in situ measurements or through comparisons between forward radiative transfer calculations using the model data and radiometer observations at frequencies up to 90 GHz. Unfortunately, the brightness temperature sensitivity to ice particles in clouds is limited by the physical and dielectric characteristics of ice for frequencies below 89 GHz. The sensitivity of higher frequency channels (> 100 GHz) to frozen particles has been proven [e.g., *Skofronick-Jackson et al.*, 2004; *Bennartz and Bauer*, 2003]. Without these higher frequencies the relationships between wide-band radiometer observations and the physical and electromagnetic properties of frozen hydrometeors cannot be determined or adequately retrieved. Understanding these physical-radiative relationships is important for developing Global Precipitation Measurement (GPM) mission satellite algorithms for the retrieval of ice characteristics both above the melting layer, as in Hurricane Erin, and for ice particles that reach the surface as falling snow.

The microphysical characteristics and high frequency radiative properties of frozen particles are complex and difficult to ascertain without detailed in situ data sets. In and above the melting layer frozen particles can range from spherical to nonspherical habits and with multiple mixtures of ice, air, and water in a single particle. The methodologies for determining the single particle and bulk layer radiative properties of frozen particles rely on several assumptions and require computationally intensive numerical models. In the past, many investigators assumed spherical particles in order to reduce modeling complexities. More recently, the radiative properties for non-spherical ice particles are being determined using the discrete dipole approximation [e.g., *Draine and Flatau*, 1994; *Liu* 2004; *Kim*, 2006] and other models [e.g., *Xu and Gustafson*, 2001].

The Fourth Convection and Moisture Experiment (CAMEX-4) provides a valuable database of active, passive, and in situ observations that is used to investigate the relationships between frozen particles and their radiative signatures. The CAMEX-4 field campaign was based in Jacksonville, Florida during August and September of 2001 [*Kakar et al.*, 2006]. This field campaign was a joint NASA and NOAA Hurricane Research Division project with the goal of studying tropical hurricane development, tracking, intensification, and land falling impacts. While remote sensing of the hurricane environment was the primary objective of CAMEX-4, there were also separate flights to study thunderstorm structure, precipitation systems, and atmospheric water vapor profiles. Multiple instruments located on ground, on low and high altitude aircraft, and on satellites were used to observe convective and hurricane systems. Of particular interest for this work are measurements from instruments on the high-altitude ER-2 aircraft at a ~20 km altitude that provide a single active radar channel and 19 passive microwave brightness temperature channels ranging from 10.7 to 183.31±10 GHz during Hurricane Erin on 10 September 2001. The higher frequency channels are extremely useful for determining and constraining the particle size distributions of the frozen hydrometeors [*Skofronick-Jackson et al.*, 2003].

The purpose of this research is to compare observed brightness temperatures to calculated brightness temperatures for several spherical and non-spherical frozen cloud hydrometeor habits in order to study how the selected ice parameterizations affect the radiative properties and resultant brightness temperatures. A radiative transfer model is employed to convert the hydrometeor parameterizations into brightness temperature values. The cloud profiles will be initialized with radar data through a conversion from reflectivity to hydrometeor content values. Other initialization procedures include determining boundary conditions and profile environmental conditions (e.g., surface wind speed and temperature, pressure, and relative humidity profiles) using dropsondes from the ER-2 and modeled Hurricane Erin data. The hydrometeor parameterizations (habits and particle size distributions for the frozen droplets) are used to compute radiative properties (absorption, scattering, and asymmetry) that are required for use in radiative transfer calculations. Then the effects of these parameterizations on the computed brightness temperatures (T_B) are compared to the observed T_B.

In section 2, details of the instruments and how the observations were co-located will be provided. The generation of the cloud hydrometeor profiles and initialization of boundary conditions will be described in Section 3. In Section 4 the radiative transfer model used in the brightness temperature calculations is summarized along with the radiative properties for each of the parameters. The comparisons between computed and observed brightness temperatures are analyzed in Section 5, followed by a summary and discussion of the key points in Section 6.

2. Observations:

While CAMEX-4 had broad-based instrumentation on multiple platforms including several aircraft and ground locations, this work focuses on the observations from four instruments on the ER-2 aircraft. On board the ER-2, flying at an altitude of approximately 20 km, the instruments of interest for this work are the High Altitude Monolithic Microwave Integrated Circuit (MMIC) Scanning Radiometer (HAMSR) [*Lambrigtsen and Riley*, 2002], the Advanced Microwave Precipitation Radiometer (AMPR) [*Spencer*, 1994], the ER-2 Doppler Radar (EDOP) [*Heymsfield et al.*, 1996], and the ER-2 dropsonde system [*Halverson, et al.*, 2004]. The first three instruments measure atmospheric hydrometeors in the microwave region of the electromagnetic spectrum, while the dropsondes are released from the ER-2 and measure temperature, relative humidity and wind speed in situ as they fall toward the Earth's surface. The HAMSR has 8 observations between 50 and 57 GHz, plus 166, 183.3±1, 183.3±1.8, 183.3±3, 183.3±4.5, 183.3±7, and 183.3±10 GHz, while the AMPR observes at the lower frequencies of 10.7, 19.35, 37, and 85.5 GHz. The EDOP is an active radar sampling at 9.6 GHz with a vertical range gate interval of 37.5 meters. HAMSR, AMPR, and EDOP are cross-track scanning instruments.

The focus is on the rain bands and anvil regions associated with Hurricane Erin on 10 September 2001. As with many Atlantic tropical cyclones, Hurricane Erin can be traced back to a tropical wave from western Africa starting 30 August 2001. Erin continued to strengthen and became a hurricane by 0000 UTC 9 September, reaching its peak intensity near 0000 UTC 10 September. On 10 September, the vertical wind shear peaked and Erin began moving over cooler waters. In response, Erin began to weaken. By 0000 UTC 15 September, Erin had turned into a tropical storm and eventually transitioned into an extratropical system. The GOES satellite image of Hurricane Erin is provided in Fig. 1 with the ER-2 aircraft flight line superimposed on top of it. The portion of the ER-2 flight line investigated in this work is identified by a thick white line in Fig. 1. The flight line begins at 33.9 N, 66.14 W and goes to 37.22 N, 63.64 W in a straight line and extends over about 450 km. Only the nadir or near-nadir signatures are used in this analysis. Figure 1 also indicates the location of dropsonde releases from the ER-2 aircraft. These were the first successful dropsonde releases from a high altitude aircraft in a hurricane [*Halverson, et al.*, 2006].

The CAMEX-4 instrument set did include the capability to measure habits and PSDs in situ. Such instruments were flown on the DC-8 aircraft with a maximum altitude of ~12 km. The in situ particle sampling instruments only obtain PSDs at the altitude of the DC-8 aircraft and spirals of the aircraft are required to get PSDs over the vertical space of the cloud. While CAMEX-4 had a few coordinated ER-2 overpasses of the DC-8 spiraling through convective clouds, unfortunately this did not occur on the 10 September 2001 flights for Hurricane Erin.

Figure 2 shows the EDOP, HAMSR, and AMPR observed data for Hurricane Erin on 10 September 2001 between 16:49:59 UTC and 17:25:00 UTC, including EDOP data (upper panel), selected HAMSR brightness temperatures (two center panels), and AMPR brightness temperatures (lower panel). For this image, the ER-2 is flying toward the northeast as indicated in Fig. 1. In the image the hurricane eye is surrounded by several rain bands with anvil, convective, and stratiform regions. From Fig. 2, it can be discerned that the higher frequencies of the HAMSR data (≥ 166 GHz) are sensitive to the frozen particles in the cloud (as indicated by non-zero reflectivities above the melting layer in the EDOP image collocated with depressions in the brightness temperatures at 166 and 183 GHz). On the other hand, the AMPR lower frequency channels are sensitive to the liquid in the rain bands. Although not readily apparent in Fig. 2, the HAMSR 50-60 GHz channels are mostly sensitive to the temperature profile.

The data sets from the AMPR, HAMSR, and EDOP have been analyzed and collocated. The largest footprint of 2.8 km occurs for the AMPR 10 and 19 GHz channels at nadir when the ER-2 is flying at 20 km altitude. Because there is not an AMPR pixel directly at nadir, the two pixels adjacent to nadir were averaged to simulate a nadir value. The HAMSR footprint resolution is about 2.0 km at nadir. However, the HAMSR data samples were separated by about 12 seconds, therefore the footprint centers were separated by about 2.5 km based on a 205 m s^{-1} aircraft speed. Since the HAMSR and AMPR footprint resolutions and locations are so similar, the collocation process was simplified. Thus, AMPR, HAMSR, and closest EDOP times were matched to the 183 points in the HAMSR data over this flight time.

3. Cloud Profile Initialization

Prior to computing brightness temperatures for these 183 observational data points, a cloud profile data set must first be generated. The radar reflectivity can provide some information about the hydrometeors, however additional data about the atmospheric profile and boundary conditions are required. There are three steps: (1) the EDOP radar reflectivities are converted into vertical hydrometeor content profiles, (2) the temperature, pressure, and relative humidity profiles need to be determined, and (3) the boundary conditions for the ocean surface and top of atmosphere must be assigned. In order to obtain the required information for steps 2 and 3, dropsonde and hurricane model data is used. The role of the dropsondes is to provide detailed information about the temperature and relative humidity profiles that is not adequately generated by the simulated Hurricane Erin.

3.1 Hydrometeor Content Profiles

Attenuation corrected [*Hitschfeld and Borden*, 1954] nadir-viewed EDOP radar reflectivity profiles are converted into estimates of hydrometeor content profiles. The fine (37.5 m) resolution of the radar range gates from 0 to ~18 km is averaged to 0.25 km vertical slabs. The hydrometeor content profiles from the radar-to-microphysical profile algorithm are partitioned into liquid and frozen particles with exponential drop size distributions, respectively. While continuity of the precipitation flux across the freezing level is not explicitly enforced, the masses obtained from the radar reflectivities have smooth transitions from one level to the next.

The averaged reflectivities are converted to rain rate using the *Marshall and Palmer* [1948] relationship:

$$M_L\,(m,h) = 0.0055(Z_{obs}(m.h))^{0.55}\ \text{g m}^{-3} \qquad (1)$$

where M_L is the mass content of the liquid particles at the flight pixel m and height level h associated with the attenuated corrected EDOP reflectivity Z_{obs} (in mm^6 m^{-3}). Once the temperature in the vertical profile reaches 0° C a portion of the content derived from Z_{obs}

is reserved for frozen particles. A linear interpolation is used to transition to all frozen hydrometeors at –22.5° C and colder. The conversion from reflectivity to frozen hydrometeor content at each level is defined by the *Sekhon and Srivastava* [1970] particle size distribution as follows:

$$M_F\,(m,h) = 0.0136\,(4.46\,Z_{obs}(m.h))^{0.39}\ \text{g m}^{-3} \qquad (2)$$

where M_F is the mass content of the frozen particles and the 4.46 factor is a correction for the frozen versus liquid particle refractive index that is usually stated as a 6.5 dBZ addition to the observed reflectivity in dBZ [*Smith*, 1984]. The transformation from reflectivities to particle contents populates the liquid and frozen hydrometeor vertical profiles.

3.2 Atmospheric Profiles

Without temperature (T), pressure (P), and relative humidity (RH) profiles, radiative transfer calculations cannot be performed. Simulated cloud fields from the Mesoscale Model-5 (MM5) of Hurricane Erin [*Wu et al.*, 2006] were used in this analysis to help generate atmospheric profiles. The MM5 model integration begins at 0000 UTC 7 September when Erin was an area of disturbed weather and was developed with a resolution of 2.0 km horizontally and ranges between 0.004 and 1.0 km vertically. The MM5 time step closest to the 10 Sept. 2001 at 1700 UTC time is selected for use within this work. The rain rate statistics of the MM5 data (without zero values included) and vertically summed liquid and frozen particle concentrations are provided in Table 1. In order to extract appropriate T, P, and RH profiles, the MM5 computed reflectivity profiles (Z_{sim}) generated by the model were compared to each of the EDOP reflectivity profiles (Z_{obs}) to generate error values (*E*):

$$E(m) = \sum_{h=o}^{cldtop} \left| Z_{sim}(i,j,h) - Z_{obs}(m,h) \right| \quad (3)$$

where m represents the mth of 183 profiles in the flight line, h is an index to the vertical profile, and i, j are indices to the MM5 output. The i, j indices associated with the five most minimum values of E for each m are used to average T and RH profiles of these five MM5 profiles for use in the radiative transfer (RT) calculations.

When these MM5 derived T and RH profiles were used in RT calculations of Hurricane Erin it became apparent that the modeled T profile at the upper altitudes was not appropriate. This was determined by reviewing the 55.5 GHz T_B channel that is sensitive to only the upper altitude temperatures. Figure 2 shows that the 55.5 GHz observations are relatively steady across the varying cloud conditions over the flight line. The computations using the MM5 generated T profiles were uniformly warm by about 5K. The inconsistency between the computed T_B using the MM5 T profile and the observations is likely attributable to the coarser vertical resolution for MM5 profiles above 300mb [*Wu et al.*, 2006]. When the MM5 temperature profiles are allowed to transition to an average (16:47:56 and 17:31:05 UTC) dropsonde profile between 7 to 18 km instead of using the MM5 temperature profiles, the comparison is much better as will be shown in Section 5. The problems in getting the calculations of 55.5 GHz to match the observations indicate a disconnect between models and observations. Furthermore, in the hurricane eye only, comparisons with the clear air 10 GHz T_B observed and computed indicated consistently too cold (MM5) computed T_B. In order to compensate for the RH and cloud water, data from dropsonde closest to the eye (1704 UTC) was employed for the temperature, pressure, and relative humidity in the first 7 km nearest the surface.

3.3 Boundary Conditions

The final step is to insert boundary conditions. For the boundary conditions at the top of the profile, the maximum height level is 18 km near the ER-2 flight altitude. Radiation from the cosmic background is incorporated in the radiative transfer calculations so that the effects of scattering from the ice at the top of the clouds are included. At the Earth's boundary an oceanic surface is assumed since the flight leg is over ocean during the focus times. The RT model requires ocean emissivity and temperature. The ocean temperature was obtained by merging dropsonde and MM5 data. Surface emissivity was more difficult to obtain since it is a function of surface roughness. The average windspeeds emanating from the MM5 data as determined by Eqn. 3 were found to be too weak to produce breaking waves with enough foam to increase emissivity and T_B warming even though Table 1 shows a maximum windspeed of 44 m s^{-1}. This discrepancy was determined using the 10 GHz channel that is sensitive to surface conditions in clear air regions. The dropsonde windspeeds were greater than those of the MM5 model and thus a linear fit between the values of the dropsonde were used, with a minimum of 8 m s^{-1} in the eye. Using the dropsonde data the windspeeds started at 20 m s^{-1} on the left hand side of the flight path, peaked at 40 m s^{-1} at the left side of the eye, dropped to 8 m s^{-1} in the eye, peaked back to 50 m s^{-1} on the right edge of the eye wall, and then transitioned to 10 m s^{-1} on the rightmost edge of the flight path. The *Monohan and Woolf* [1989] static foam model worked best in generating realistic foam amounts for ocean surface emissivity computations.

4. Particle Habit and Parameterizations

The frozen cloud particle contents (in g m^{-3}) derived from the EDOP reflectivities are partitioned into three different frozen habits and exponential particle size distributions (PSDs) in order to compute the electromagnetic absorption, scattering, and symmetry factors of the frozen particles required for brightness temperature computations. These factors describe how the incident radiation will be absorbed and scattered. The emissive properties of the ocean surface and raindrops are also incorporated. The first habit uses the solid spherical ice *Sehkon and Srivastava* [1970] PSD, while the second habit assumes a dry fluffy spherical snow particle. The third parameterization assumes a three dimensional bullet rosette of three columns intersecting at orthogonal angles at their center points, like an X-Y-Z axis intersection. The *Marshall-Palmer* [1948] remains constant as the liquid PSD for all three frozen habit cases.

Since detailed in situ habits and PSDs were not measured for this CAMEX-4 ER-2 flight, the three frozen habits and PSD (or microphysical) parameterizations were selected from published literature in order to compare how changes in the PSD and habit for frozen hydrometeors affect the computed T_B and the comparison with the observed T_B. While this is a qualitative comparison it still reveals information about the applicability of the different frozen parameterizations with respect to the CAMEX-4 Hurricane Erin observations and different portions of the storm.

All of the three frozen habits employ polydispersive particle size distributions. The absorption and scattering coefficients for each layer and hydrometeor are determined by integrating over the polydispersive particle size distributions. For all parameterizations, the PSD, or number density of the particles within the diameter range D to $D + dD$, is modeled by a decaying inverse exponential function:

$$N(D) = N_0 \exp(-\Lambda D) \quad (4)$$

where N_0 is a multiplier in $m^{-3}mm^{-1}$ and $\Lambda=(2<r>)^{-1}$ in mm describes the average radius size parameter. At each height interval, the relationship between the bulk (summed) scattering coefficient and bulk absorption coefficient can be used to indicate if radiative cooling from scattering or warming from absorption will dominate. The asymmetry factor describes the direction(s) of scattering with values close to +1 indicating forward scattering, those close to -1 backward scattering, and those at zero indicating isotropic scattering.

4.1 Parameterization 1

Here the frozen droplets use a fluffy particle PSD [*Tao and Simpson*, 1993]. The particles are assumed to be 10% ice and 90% air with

$$N_{0fluffy} = 4000.0 \text{ m}^{-3} \text{ mm}^{-1} \quad (5)$$

$$\Lambda_{fluffy}^{-1} = \frac{M}{\pi \rho_{fluffy} N_{0fluffy}} \text{ mm} \quad (6)$$

where ρ_{fluffy} = 0.1×10^6 g m^{-3} for 10% ice. The particles are spherical in shape. The Maxwell-Garnett [*Bohren and Battan*, 1980] dielectric mixing theory is used to obtain the refractive index of these mixed phase (ice and air) particles and then Mie theory is used to determine the absorption, scattering, and asymmetry factors for the RT computations. The particles are allowed to extend to a maximum size of about 10 mm with N(D) on the order of 10^{-1} at this maximum size and for M = 1 g m^{-3}.

4.2 Parameterization 2

For the second parameterization, the frozen drops follow that of the *Sehkon-Srivastava* [1970] PSD, denoted SS. The SS PSD assumes solid ice spheres for the frozen droplets. These were the size distributions used in Equation 2 to convert reflectivity to hydrometeor ice content. The Λ and N_0 in Eqn. 4 are:

$$N_{0SS} = 636.38\, M^{1.093}\ \mathrm{m^{-3}\ mm^{-1}} \tag{7}$$

$$\Lambda_{SS}^{-1} = 1.185\, M^{-0.524}\ \mathrm{mm} \tag{8}$$

where M is the ice content in g m^{-3} in each cloud layer interval. The refractive index for solid ice [*Warren*, 1984] is used in the Mie expressions for determining the radiative properties. In the PSD the maximum size is 10 mm where the N(D) is 10^{-2} for M values of 1.0 g m^{-3}.

4.3 Parameterization 3

This third parameterization has a habit similar to a bullet rosette with three cylinders intersecting at their center points and is denoted C3. This habit was described in *Kim* [2006], with the single cylinder aspect ratio from *Auer and Veal* [1970] and *Kim et al.* [2007]:

$$D = 0.197 L^{0.414}\ \text{(mm)} \tag{9}$$

where L is the length and D is the diameter of the column. The Λ in Eqn. 4 is a function of the temperature as it varies over the profile height and comes from *Lo and Passarelli* [1982]:

$$\Lambda_{C3}^{-1} = 10^{-T/41} \tag{10}$$

where T is in Celsius. The maximum size of the particle size distribution is fixed by Kim 2006 requiring that the size parameter ($\pi D_{eff}\ \lambda^{-1}$) < 2.5 where λ is the operational wavelength and D_{eff} which is the effective diameter of a spherical particle with volume given by the three intersecting cylinders. Note that we plotted *Kim's* [2006] provided curve fits and determined that they were good up to size parameters of 3.5. Thus the maximum L for this PSD is 7 mm. At 7 mm the N(D) value is on the order of 10^{-4}, while for 5 mm N(D) is closer to 10^{-2} for T = -20°C and M = 1 g m^{-3}.

The volume for the 3 cylinder habit is given by:

$$V = \frac{3}{4}\pi D^2 L - \sqrt{2}D^3 \qquad (11)$$

where the intersecting center volume is removed for two of the cylinders. The Λ_{C3} is determined using Eqn. (10). The habit shape and aspect ratio fixes the volume in each individual particle such that given the maximum diameter the total ice water content (M) in each layer can be partitioned into an exponential particle size distribution and N_0 can be determined using Eqn (11). The increment in the L dimension for the particle size distribution is 0.1 mm.

In order to compute the absorption, scattering, and asymmetry parameters for these non-spherical particles, Mie theory is used for frequencies less than 80 GHz [*Kim*, 2006]. For frequencies above 80 GHz, the discrete dipole approximation is used [*Draine and Flatau*, 1994]. The procedure is similar to that described in *Kim* [2006] and the DDA curve fit coefficients for this aspect ratio are provided in Table 2. The curve fit equations are from *Kim* [2006] and are reproduced here:

$$\log_{10}\left(\frac{C_{scat}}{\pi r_{eff}^2}\right) = \sum_{n=0}^{7} A_n \left(\log_{10} x\right)^n \qquad (12)$$

$$\frac{C_{abs}}{\pi r_{eff}^2} = \sum_{n=0}^{5} B_n x^n \qquad (13)$$

$$\log_{10}(g) = \sum F_n (\log_{10} x)^n \ . \qquad (14)$$

To provide proper disclosure, the resultant brightness temperatures are relatively sensitive to the habit and the prescribed PSD. For example, a single column habit produced warmer brightness temperatures than this three intersecting column habit. Further, changing the aspect ratio of the individual columns does affect the radiative properties. Finally, we have imposed a PSD [*Lo and Passarelli*, 1982] though we have noted that changing the $\Lambda(T)$ will affect the brightness temperatures as well.

5. Radiative Transfer Calculations

An accurate and efficient radiative transfer (RT) model is required to transform the microphysical information into upwelling passive microwave brightness temperatures (T_B) that are then compared to the AMPR and HAMSR observations. The radiative transfer model used in this work is a planer-stratified scattering based model originally developed by *Gasiewski* [1993] and modified as described in *Skofronick-Jackson et al.*, [2003]. The RT model used herein allows for multiple scattering among the six different hydrometeor types (i.e., suspended cloud water, rain, suspended cloud ice, snow, hail, and graupel). In this work only rain and snow are allowed, though the size distributions for rain and snow extend down to sizes appropriate for cloud water and cloud ice. Flexibility exists in that the user can select observation height, viewing angle, frequency (tested from 6 to 425 GHz) and polarization. The RT model requires as input instrument specifications, vertical profiles of temperature, height, relative humidity, and PSDs of the hydrometeors in the cloud or their radiative properties. It is assumed that a planar stratified RT model is acceptable in this work since only high resolution nadir observations are used in the retrieval. Furthermore, since only nadir observations are analyzed in this work, any polarization sensitivity due to nonspherical particles is minimized.

Once individual absorption, scattering, and asymmetry factors have been computed for each shape as described in Section 4, they are integrated over polydispersive PSDs as described in *Gasiewski* [1993] to obtain the bulk absorption, scattering, and asymmetry factors over the vertical structure of the hurricane flight line. Figure 3 shows the bulk absorption coefficients for the three different frozen habits at 183±7 GHz, while Figure 4 provides the scattering coefficients. There is essentially no difference in the absorption profiles since the Marshall-Palmer PSD for rain was not changed and ice particle do not contribute much to the absorption coefficient. For the scattering profiles, the fluffy and rosette habits tend to produce a bit more scattering than the SS case. Scattering is increased for the fluffy by its relatively large particle size and larger N(D) at those larger sizes. For the rosette habit, scattering is larger than that of the SS particles but less than that of the fluffy particles because of its intermediate size and N(D) values.

On the other hand, the asymmetry parameters at 183±7 GHz (and for each frequency in turn) are very different for the three cases (Figure 5). For fluffy spheres, the asymmetry is above 0.8 for the highest altitudes (Fig. 5a) and closer to 0.5 in the midaltitude range. For the solid ice sphere (SS) case, the asymmetry factors are near 0.4 to 0.6 in most of the liquid and frozen parts of the vertical profile. On the other hand, the three-dimensional rosette particle has asymmetry values decreasing with altitude (Fig. 5c). Since an asymmetry factor of +1.0 is pure forward scattering, the fluffy spheres allow the warm emission from rain and the Earth's surface to forward scatter into the radiometer and the cold cosmic background to forward scatter to lower layers, hence producing warmer brightness temperatures. For the SS shapes, the asymmetry factor shows a slight preference for forward scattering, but a bit more isotropic. Thus because of multiple scattering effects, radiation is scattered such that the resulting effect for the SS shape is cold brightness temperatures. Finally, for the three-dimensional rosette particles, the asymmetry factor is similar to the asymmetry of the SS particles except that it goes to close to zero at the top of the cloud. This is because Λ_{C3} is a function of temperature and hence so is the average particle size at each temperature layer. This means that at the top of the cloud, where the radiometer will receive most of the signal, particles are small and scattering is isotropic, so the radiometer senses both warming from rain and/or surface emission and cooling from cold cosmic background and the upper cloud layers. Because the cold upper layers are closer to the radiometer, they have a larger impact in cooling the radiometer brightness temperatures.

At 85 GHz, the absorption fields for the three parameterizations are as equivalent as in the 183 GHz case. On the other hand the scattering profiles (Fig. 6) show that only the SS parameterization has significant scattering in the ice layers. In Fig. 7, the 85 GHz asymmetry shows a pattern similar to the 183 GHz asymmetry but at lower and more isotropic values.

Although not shown, for 166 GHz the absorption, scattering, and asymmetry factors have similar patterns as at 183 GHz. At 10 GHz the asymmetry factor ranges between -0.05 and 0.2 for all three frozen habits. This means that any 10 GHz scattering (also less than ~0.25 neper km^{-1} for all habits) is more isotropic, however at 10 GHz the strong absorption coefficient overpowers the weak scattering signal.

6. Comparison between Observed and Computed Brightness Temperatures

The radiative transfer model along with the computed bulk radiative data were used to compute brightness temperature values for the three ice parameterizations. These values for many of the frequencies are presented in Figures 8, and 9. Prior to comparing observations to the calculations, a review of Figure 2 will show that the cloud structures are quite variable in several sections of the ER-2 flight line and these will cause some discrepancies between the observations and the calculations in these regions since the microphysical properties are apt to be quite variable as well. Specifically, time frames of 16:58 UTC through 17:04 UTC and about 17:15 UTC and 17:20 UTC near the transitions between inner and outer hurricane rain bands are highly variable. Note that in the hurricane eye all three parameterizations produce equivalent computed brightness temperature values. This means that differences in T_B outside the eye are due to the differences in the three frozen parameterizations.

In general, the fluffy particles did not produce enough scattering and proper asymmetry directions to reduce calculated brightness temperatures to the lower observed values at the higher frequencies. On the other hand, the solid ice sphere (SS) produced excessive scattering in some locations. The three-dimensional rosettes managed to reasonably capture the observed AMSR and HAMSR brightness temperatures. In the following paragraphs the results for the different parameterizations will be discussed for each plotted frequency.

For 10 GHz, all three parameterizations track the observations along the flight line reasonably well and are within ~10K except in the eye of Hurricane Erin. While the corrections in surface windspeed and near surface temperature and relative humidity profiles did warm 10 GHz by ~10-20 K (see section 3.3), additional measures are necessary. Perhaps wind driven foam persists even the calm of the eye. This is a future research topic.

For 19 GHz, there is a similar response as for 10 GHz. For both 19 and 10 GHz, brightness temperature calculations near the regions of a clearly defined radar bright band (horizontal red lines in Figure 2, EDOP image) are depressed with respect to the observations. This may indicate that the Marshall-Palmer PSD used for rain and/or the vertical transitions between all rain and all ice are inadequately modeled. For 19 GHz adding a melting layer would warm the T_B values by 2-3 Kelvin [*Skofronick-Jackson et al.*, 2002].

For 37 GHz the calculations for all parameterizations track the observations, except near the Hurricane Erin's eye (as for 10 and 19 GHz). There is more variability among the three parameterizations since 37 GHz is sensitive to both ice and rain particles. In this region, Hurricane Erin and the microphysical profile is complex with ice aloft separated from rain below with clear air between. This type of cloud structure is extremely difficult to appropriately model. For 37 GHz, adding a melting layer would have the largest impact where T_B values are increased by up to 5-15 K [*Skofronick-Jackson et al.*, 2002].

For 55.5 GHz the brightness temperatures do not change by more than 5-6 Kelvin across the whole flight line observations due to the fact that this channel is sensitive to temperatures high in the atmosphere, closest to the ER-2 aircraft. Since the sensitivity altitude exists above any hydrometeors, there is little response of this channel to hydrometeors. As noted in Section 3.2, the MM5 generated T profiles were replaced by the colder profiles from the dropsondes. This was required to get the 55.5 GHz T_B calculations closer to the observations.

For 85 GHz in Figure 8, brightness temperatures from the three parameterizations show more deviations. This is expected since the three parameterizations differ only in their frozen particle characteristics and 85 GHz is responsive to frozen hydrometeor characteristics. Here the SS habit causes too much cooling due to high scattering and the nature of its asymmetry factor. The fluffy particles have relatively low scattering and high asymmetry such that warming from lower absorptive layers is reflected in the warmer TB values. For the rosette particles, 85 GHz scattering is almost non-existent and asymmetry is mostly isotropic (see Fig. 6 and 7), which means there is little contribution of cooling from ice scattering at 85 GHz for the rosette particles. It is likely that adding a melting layer would increase T_B values by ~5-10K [*Skofronick-Jackson et al.*, 2002] which is the wrong direction of change if the goal is to cool calculations to match the observations. The most likely cause of the discrepancy for the computed T_B with respect to the observed T_B is that the rosette, fluffy, and SS particles are not typical particles that exist at the mid-levels at 85 GHz senses. This means that the vertical distribution of PSDs (and hence average particle size) is not yet appropriate for the mid-level particle that 85 GHz senses.

In the first panel of Figure 9, the 166 GHz channel image is shown. The 166 GHz channel is a window channel like 85 GHz, however it responds to ice particles smaller and at a higher altitude than those sensed by the 85 GHz channel due to its smaller operating wavelength. For the 166 GHz channel, the rosette habit and its PSD produces a better match to the observations than do the other parameterizations.

In Figure 9 some of the 183 GHz water vapor channel series of the HAMSR instrument are shown. As the channels move from 183±1 to 183±10 GHz the sensitivity moves from the top of the cloud to lower altitudes in the cloud. In the absence of clouds these channels respond to the water vapor in clouds and are used to estimate water vapor profiles. When clouds are present, these channels respond to the frozen hydrometeors mostly, since these channels have a small operating wavelength and become saturated quickly in the presence of particles with diameters near the operating wavelength.

In each of the comparisons between observation and calculations for the 183 GHz channels, the best parameterization appears to be the one employing the C3 rosette particles and the *Lo and Passarelli* [1982] PSD. The SS parameterization causes too much scattering, while the fluffy particles do not provide enough scattering and proper asymmetry directions at these higher frequencies. The effective dielectric mixing theories [*Bohren and Battan*, 1980] used for the fluffy particles assume that the size of the inclusion is much smaller than the wavelength of the radiometer frequency [*Sihvola*, 1989]. Using these models for the higher frequencies seemed to produce inappropriate electromagnetic characteristics. For example, the fluffy particles represented by effective medium mixing models did not have cold enough T_B because the asymmetry factor was too large. As stated previously, the asymmetry factor is a function of the particle shape, size, temperature, and ice-air-water composition and determines the direction(s) of scattering from a hydrometeor. Large asymmetry factors increased forward scattering of the radiation from the warm lower layers so that computed brightness temperatures were too warm. The C3 rosette shape along with the discrete dipole approximation along with the *Lo and Passerelli* [1982] PSD produced the scattering and asymmetry factors that led to the T_B computations closest to the observations.

7. Summary and Conclusions

This work was undertaken in order to evaluate the relationships between frozen cloud particles and their radiative signatures for improving algorithm development of ice particle characteristics (for falling snow retrievals and hurricane intensity assessments.) In summary, three different ice parameterizations were used to compute brightness temperature values to compare with observations from CAMEX-4 radiometers on the ER-2 aircraft. In order to initialize the cloud profiles used in the radiative transfer calculations, the radar reflectivities taken from the EDOP instrument on the ER-2 were converted to mass contents at 0.25 km interval levels from 0.25 km to 18 km in the vertical profile. The EDOP reflectivities were compared to Hurricane Erin MM5 modeled reflectivities to extract and average the five closest atmospheric profiles such that the MM5 profiles of temperature, pressure, and relative humidity were available across the ER-2 flight path data set. Surface wind speeds and ocean surface temperature are similarly generated. The MM5 generated temperature profiles above 7.5 km were replaced by the dropsonde data due to coarse sampling in the upper altitude MM5 modeled profiles that caused inconsistencies in the frequency (55.5 GHz) sensitive to high altitude temperature profiles. Surface windspeeds are similarly interpolated from the dropsonde data.

With the profile database generated by the EDOP instrument, dropsondes, and the Hurricane Erin MM5 model, brightness temperatures were computed for the three ice parameterizations. The liquid drops followed the *Marshall and Palmer* [1948] PSD throughout all parameterizations. The first parameterization relied on the *Sehkon and Srivastava* [1970] PSD for ice particles, the second parameterization relied on fluffy (10% ice, 90% air) particles, while the third parameterization was of a three-dimensional bullet rosette particle of three intersecting cylinders in a polydispersive size distribution.

In comparing the observations to the calculations, the overall best fit resulted from the rosette particles of three intersecting cylinders. The fluffy did not produce the cold scattering signatures caused by ice that was measured in the observations. This indicates inadequate modeling of its scattering and asymmetry electromagnetic characteristics likely caused by representing them as fluffy, 10% ice spheres.

As would be expected, the lower frequency AMPR observations (10 to 19 GHz) had essentially no difference among the three parameterizations (Figure 8). These channels are mostly responsive to the liquid particles in the cloud and the parameterizations discussed herein only made changes to the frozen droplets. At 37 GHz, we expect and note a response to both liquid and frozen particles. The 50 to 60 GHz band of the HAMSR instrument is typically used for temperature profiling with the lower frequencies sensing more about the lower altitudes and vice-versa for the slightly higher frequencies. These temperature profiling channels are responsive to hydrometeors in the cloud except at the higher frequencies close to 60 GHz that sense only high altitude atmospheric temperatures. The 183 GHz channels are sensitive to both atmospheric water vapor and the frozen droplets in the cloud. The SS parameterization tended to overemphasize the scattering and caused T_B that were too cool with respect to the observations, while the bullet rosette (three cylinder) T_B values more closely match these high frequency observations. Using rosette particles in the RT calculations matched all frequencies except at 85 GHz where calculations were too warm. This is likely caused by complex microphysical variations in the frozen particle habit and its PSD that is poorly modeled across the vertical profile.

The four most significant findings of this work are summarized here. The first finding was that the MM5 cloud model did not have enough vertical resolution at its highest altitudes to produce the temperature profiles needed to compute T_B in the 55 to 60 GHz range and hence coincident dropsonde data was required. The second significant finding was the ocean surface conditions were difficult to ascertain in the hurricane eye so that brightness temperatures that depended on the surface conditions did not match the observations well. The third finding revealed the importance of the bulk asymmetry parameter (that describes the direction of scattering) in the resultant T_B values. Typically, passive remote sensing has attributed T_B values to the combination of the bulk absorption and scattering parameters, essentially ignoring the role of the asymmetry. The fourth and most important finding was that non-spherical particles, in this case modeled as bullet rosettes, provided the absorption, scattering, and asymmetry radiative properties that when used in the radiative transfer calculations gave the best match to the observations.

This work has shown that the full channel spectrum of electromagnetic properties of frozen hydrometeors is difficult to model using a single simplified parameterization and that the bulk asymmetry factor plays a big role in the resultant computed high frequency brightness temperatures. In likelihood, multiple habit and PSD models will be required. These physical models will depend on many factors such as vertical location and atmospheric temperature, method of forming and re-freezing, and ice-air-water ratios. Detailed in situ observations and reliable cloud resolving models for the ice phase particles are required in order to develop and validate appropriate and more universal frozen particle parameterizations for radiative transfer calculations. Meanwhile this work shows that some early non-spherical models such as the three-dimensional bullet rosette with three intersecting cylinders can produce brightness temperatures comparable to most wideband passive observations.

Acknowledgments

We wish to thank the Global Hydrology Center at NASA Marshall Space Flight Center for providing the instrument data at a unified webpage. We also thank the instrument Principal Investigators Dr. Jeff Halverson for the dropsonde data, Dr. Gerald Heymsfield for the EDOP data, Robbie Hood for the AMPR data, and Dr. Bjorn Lambrigtsen for the HAMSR data. We wish to thank Drs. Scott Braun and Liguang Wu for the MM5 simulated data. We thank Ben Johnson and Faith Collins for helpful discussions and studies that supported this work. We acknowledge the Missouri Space Consortium and NASA Goddard for summer student support of Eric Holthaus and Cerese Albers. Interest in our work by Dr. Ramesh Kakar of Code Y at NASA HQ is also gratefully appreciated.

References:

Auer, A. H., and D. L. Veal (1970), The dimension of ice crystals in natural clouds, *J. Amos. Sci.*, *27*, 919-926.

Bennartz, R. and P. Bauer (2003), Sensitivity of microwave radiances at 85 183 GHz to precipitating ice particles, *Radio Science*, *38*(4), 8075, doi:10.1029/2002RS002626.

Bohren, C. F., and L. J. Battan (1980), Radar backscattering by inhomogeneous precipitating particles. *J. Atm. Sci.*, *37*, 1821-1827.

Draine, B. T., and P. J. Flatau (1994), Discrete dipole approximation for scattering calculations, *J. Opt. Soc. Am.*, *A11*, 1491-1499.

Gasiewski, A. J. (1993), Microwave radiative transfer in hydrometeors, in *Atmospheric Remote Sensing by Microwave Radiometry*, edited by M. A. Janssen, pp. 91-144, John Wiley and Sons.

Halverson, J.B., J. Simpson, G. Heymsfield, H. Pierce, T. Hock, and L. Ritchie (2006), Warm core structure of Hurricane Erin diagnosed from high altitude dropsondes during CAMEX-4, *J. Atmos. Sci.*, *63*, 309-324.

Heymsfield, G. M., S. Bidwell, I. J. Caylor, S. Ameen, S. Nicholson, W. Boncyk, L. Miller, D. Vandemark, P. E. Racette, and L. R. Dod (1996), The EDOP radar system on the high-altitude NASA ER-2 aircraft, *J. Atmos. Ocean. Tech., 13,* 795-809.

Heymsfield, A. J, A. Bansemer, S. L. Durden, R. L. Herman, and T. P. Bui (2006), Ice microphysics observations in Hurricane Humberto: Comparison with non-hurricane generated ice cloud layers, *J. Atmos. Sci.*, *63*, 288-308.

Hitschfeld, W. and J. Bordan (1954), Errors inherent in the radar measurement of rainfall at attenuating wavelengths, *J. Meteor.*, *11*, 58-67.

Kakar, R., M. Goodman, R. Hood, and A. Guillory (2006), Overview of the Convection and Moisture Experiment (CAMEX), *J. Atmos. Sci.*, *63*, 5-18.

Kim, M.-J. (2006), Single scattering parameters of randomly oriented snow particles at microwave frequencies, *J. Geophys. Res.*, *111*, D14201, doi:10.1029/2005JD006892.

Kim, M.-J., J. A. Weinman, W. S. Olson, D.-E. Chang, G. Skofronick-Jackson, and J. R. Wang (2007), A Physical Model to Estimate Snowfall over Land using AMSU-B Observations, Submitted to *J. Geophys. Research*, March 2007.

Lambrigtsen, B. H. and A. L. Riley (2002), Microwave Scattering Observed in Convective Cells During CAMEX-4. Proceedings AMS 25th Conference on Hurricanes and Tropical Meteorology; San Diego, CA, 13A.6.

Liu, G. (2004), Approximation of single scattering properties of ice and snow particles for high microwave frequencies, *J. Atmos. Sci.*, *61*, 2441 2456.

Lo, K. K. and R. E. Passarelli (1982), The growth of snow in winter storms: An airborne observational study, *J. Atmos. Sci.*, *39*, 697-706.

Marshall, J. S. and W. M. Palmer (1948), The distribution of raindrops with size, *J. Meteor.*, *5*, 165-166.

McFarquhar, G. M., H. Zhang, G. Heymsfield, R. Hood, J. Dudhia, J. B. Halverson, and F. Marks Jr. (2004), Factors affecting the evolution of Hurricane Erin and the distributions of hydrometeors: Role of microphysical processes. *J. Atmos. Sci.*, *63*, 127-150.

Monahan, E. C. and Woolf, D. K. (1989), "Comments on "Variations of Whitecap Coverage with Wind Stress and Water Temperature" ", *J. Phys. Oceanogr. 19*, 706 709.

Sehkon, R. S. and R. Srivastava (1970), Snow size spectra and radar reflectivity, *J. Atmos. Sci.*, *27*, 299-307.

Sihvola, A.H. (1989), Self-consistency aspects of dielectric mixing theories, *IEEE Trans. on Geosci. and Remote Sens.*, *27*, 403-415.

G. M. Skofronick-Jackson, A. J. Gasiewski, and J.R. Wang, 2002: Influence of microphysical cloud parameterizations on microwave brightness temperatures," *IEEE Trans. Geosci. and Remote Sensing*, *40*, 187-196.

Skofronick-Jackson, G. M., M. J. Kim, J. A. Weinman, and D. E. Chang (2004), A physical model to determine snowfall over land by microwave radiometry, *IEEE Trans. Geosci. Remote Sens.*, *42*, 1047-1058.

Smith, P. L. (1984), Equivalent radar reflectivity factors for snow and ice particles, *J. Clim. Appl. Meteorol.*, *23*, 1258-1260.

Spencer, R.W., R.E. Hood, F.J. LaFontaine, E.A. Smith, R. Platt, J. Galliano, V.L. Griffin, and E. Lobl (1994), High-resolution imaging of rain systems with the advanced microwave precipitation radiometer, *J. Atmos. Ocean. Tech.*, *11*, 849-857.

Tao, W.-K., J. Shi, S. Chen, S. Lang, S.-Y. Hong, C. Peters-Lidard, S. Braun, and J. Simpson (2007), Revised bulk-microphysical schemes for studying precipitation processes. Part I: Comparisons with other schemes, Submitted to *Mon. Wea. Rev.* February 2007.

Tao, W.-K., and J. Simpson (1993), Goddard Cumulus Ensemble Model. Part I: Model description, *Terrestrial, Atmospheric, and Oceanic Sciences*, *4*, 35-72.

Warren, S. G. (1984), Optical constants of ice from the ultraviolet to the microwave, *Appl. Optics*, *23*, 1206 1225.

Willoughby, H.E. (1998), Tropical cyclone eye thermodynamics, *Mon. Wea. Rev.*, *126*, 3053-3067.

Wu, L., S. A. Braun, J. Halverson, G. Heymsfield (2006), A Numerical Study of Hurricane Erin (2001). Part I: Model Verification and Storm Evolution, *J. Atmos. Sci.*, *63*, 65-86.

Xu y.-L. and B.A.S, Gustafson (2001). A generalized multiparticle mie-solution: Further experimental verification, *JQSRT*, *70*, 395-419.

Figure Captions:

Figure 1: Visible GOES image with 10 September 2001 ER-2 aircraft flight track superimposed. The flight line of interest in this work is identified with a thick white line with an arrow showing flight direction. Stars indicate three dropsonde release locations.

Figure 2: Collocated EDOP-HAMSR-AMPR Hurricane Erin data set from 10 September 2001.

Figure 3: Bulk absorption fields at 183±7 GHz for (a) fluffy spheres, (b) solid ice SS spheres, and (c) three-dimensional rosettes. Shading thresholds are at 0.1, 0.5, 1.0, and 2.0 nepers/km.

Figure 4: Bulk scattering fields at 183±7 GHz for (a) fluffy spheres, (b) solid ice SS spheres, and (c) three-dimensional rosettes. Shading thresholds are at 0.1, 0.5, 1.0, 2.0, 3.0, and 4.0 nepers/km.

Figure 5: Bulk asymmetry fields at 183±7 GHz for (a) fluffy spheres, (b) solid ice SS spheres, and (c) three-dimensional rosettes. Asymmetry factors are unitless.

Figure 6: Bulk scattering fields at 85 GHz for (a) fluffy spheres, (b) solid ice SS spheres, and (c) three-dimensional rosettes. Shading thresholds are at 0.1, 0.5, 1.0, 2.0, 3.0, and 4.0 nepers/km.

Figure 7: Bulk asymmetry fields at 85 GHz for (a) fluffy spheres, (b) solid ice SS spheres, and (c) three-dimensional rosettes. Asymmetry factors are unitless.

Figure 8: Brightness temperature values for 10, 19, 37, 55.5, and 85 GHz in Kelvin for the observations (solid line), SS parameterization (dotted line), Fluffy parameterization (dashed line), and rosette parameterization (dash-dotted line).

Figure 9: Same as Figure 6 except for 166, 183.3±1, ±3, ±7, and ±10 GHz.

Field	Average	Median	Maximum
Surface Rain Rate (mm hr^{-1})	4.8	0.2	19.1
Liquid Profile Total (g m^{-3})	3.5	0.9	69.5
Ice Profile Total (g m^{-3})	1.6	0.5	36.1
Surface Wind Speeds (m s^{-1})	20.09	19.5	44.8

Table 1: MM5 Model statistics, zero values not included in average.

	Scattering Coefficient		Asymmetry Coefficient		Absorption Coefficient 85 GHz	Absorption Coefficient 166 GHz	Absorption Coefficient 183 GHz
A_0	-0.4732	**F_0**	-0.3464	**B_0**	1.5E-04	1.1E-04	-6.6E-04
A_1	2.7905	**F_1**	0.9238	**B_1**	0.0021	0.0061	0.0153
A_2	-0.7234	**F_2**	-1.9033	**B_2**	0.0081	0.0086	-0.0032
A_3	0.8752	**F_3**	1.5002	**B_3**	-0.0051	-0.0022	0.0062
A_4	-0.8767	**F_4**	2.7539	**B_4**	0.002	5.35E-4	-0.0014
A_5	-3.5739	**F_5**	-1.8551	**B_5**	-2.6E-04	-4.8E-05	8.5E-05
A_6	-2.6398	**F_6**	-3.6527	-	-	-	-
A_7	-0.6078	**F_7**	-1.2428	-	-	-	-

Table 2: Fitting Coefficients for equations 12, 13, and 14.

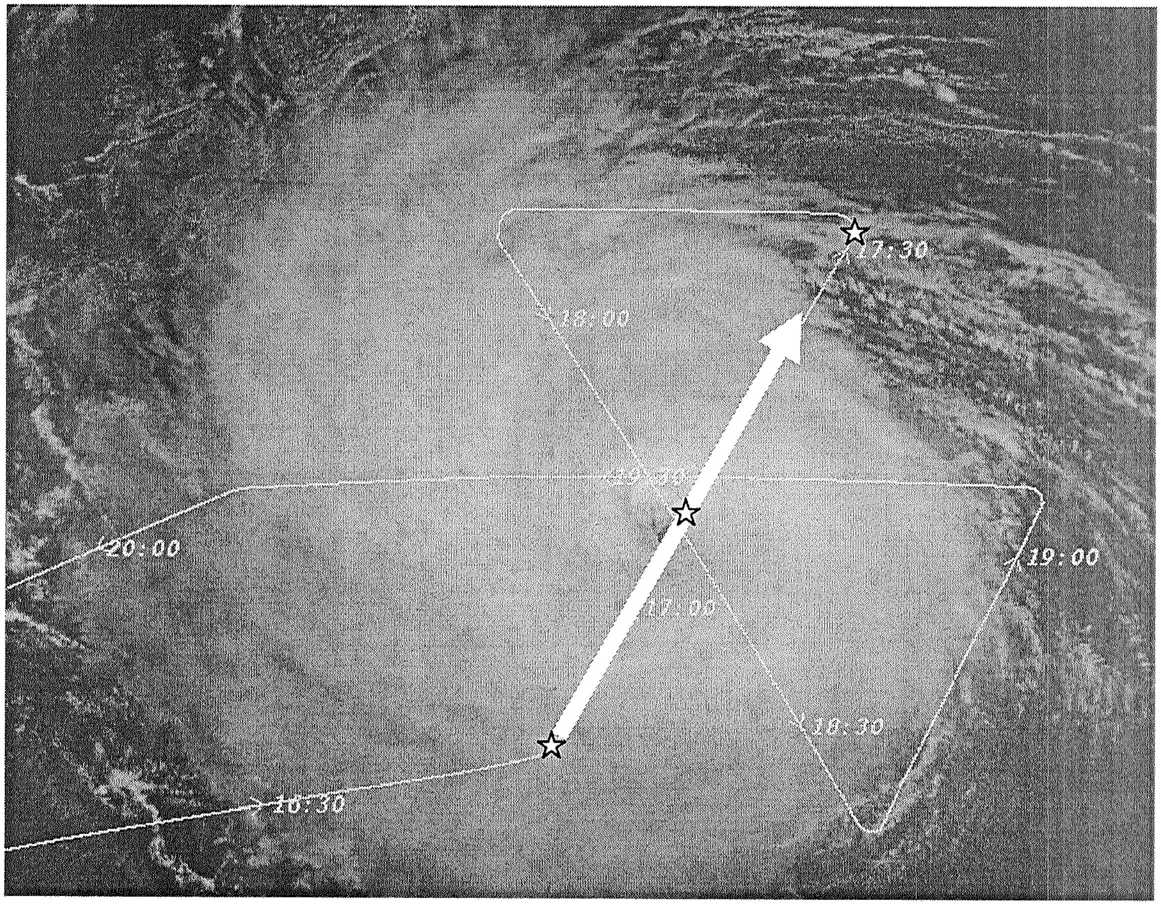

Figure 1: Visible GOES image for 10 September 2001 at 17:01 UTC with 10 September 2001 ER-2 aircraft flight track superimposed. The flight line of interest in this work is identified with a thick white line with an arrow showing flight direction. Stars indicate three dropsonde release locations.

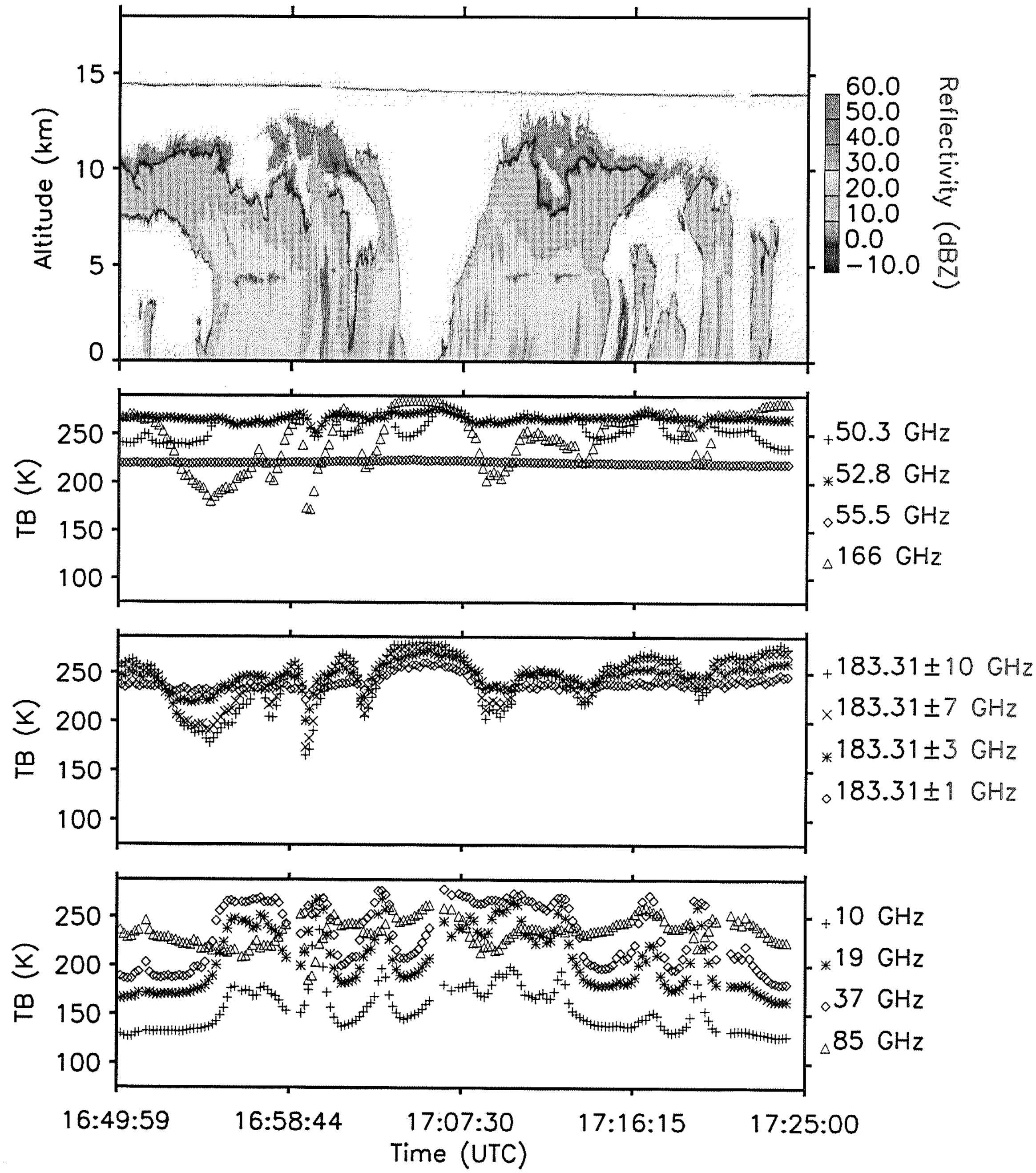

Figure 2: Collocated EDOP-HAMSR-AMPR Hurricane Erin data set from 10 September 2001.

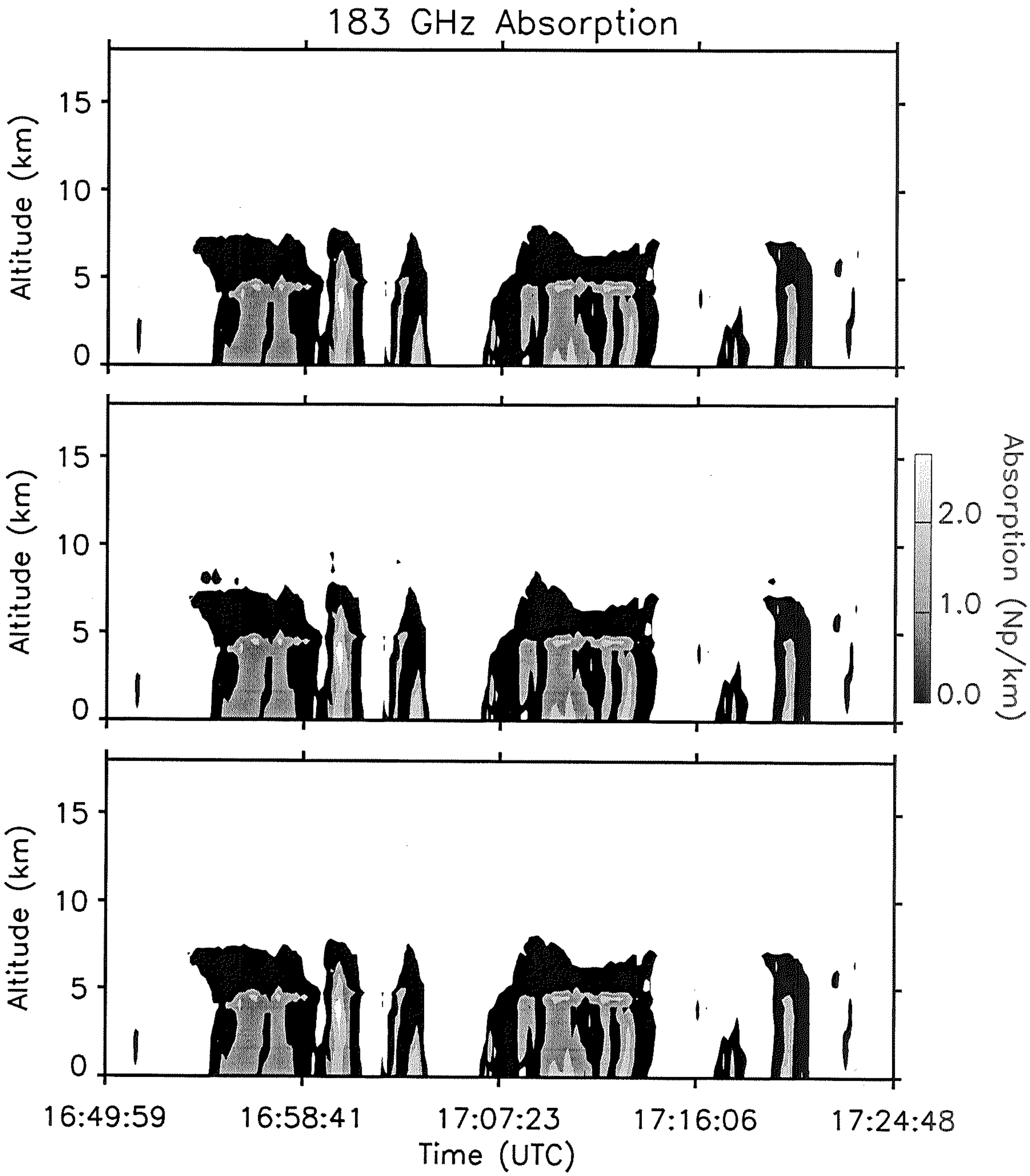

Figure 3: Bulk absorption fields at 183±7 GHz for (a) fluffy spheres, (b) solid ice SS spheres, and (c) three-dimensional rosettes. Shading thresholds are at 0.1, 0.5, 1.0, and 2.0 nepers/km.

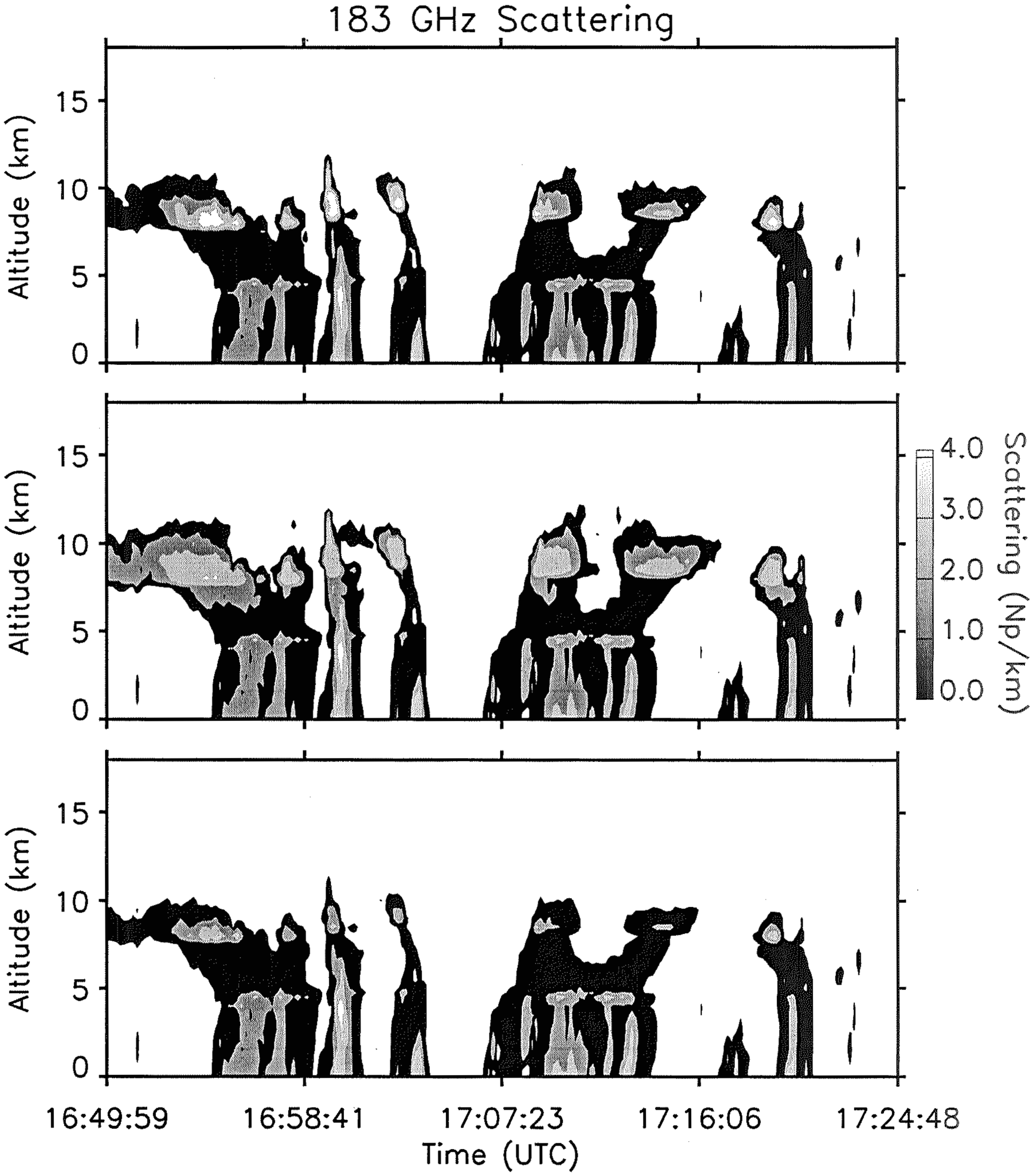

Figure 4: Bulk scattering fields at 183±7 GHz for (a) fluffy spheres, (b) solid ice SS spheres, and (c) three-dimensional rosettes. Shading thresholds are at 0.1, 0.5, 1.0, 2.0, 3.0, and 4.0 nepers/km.

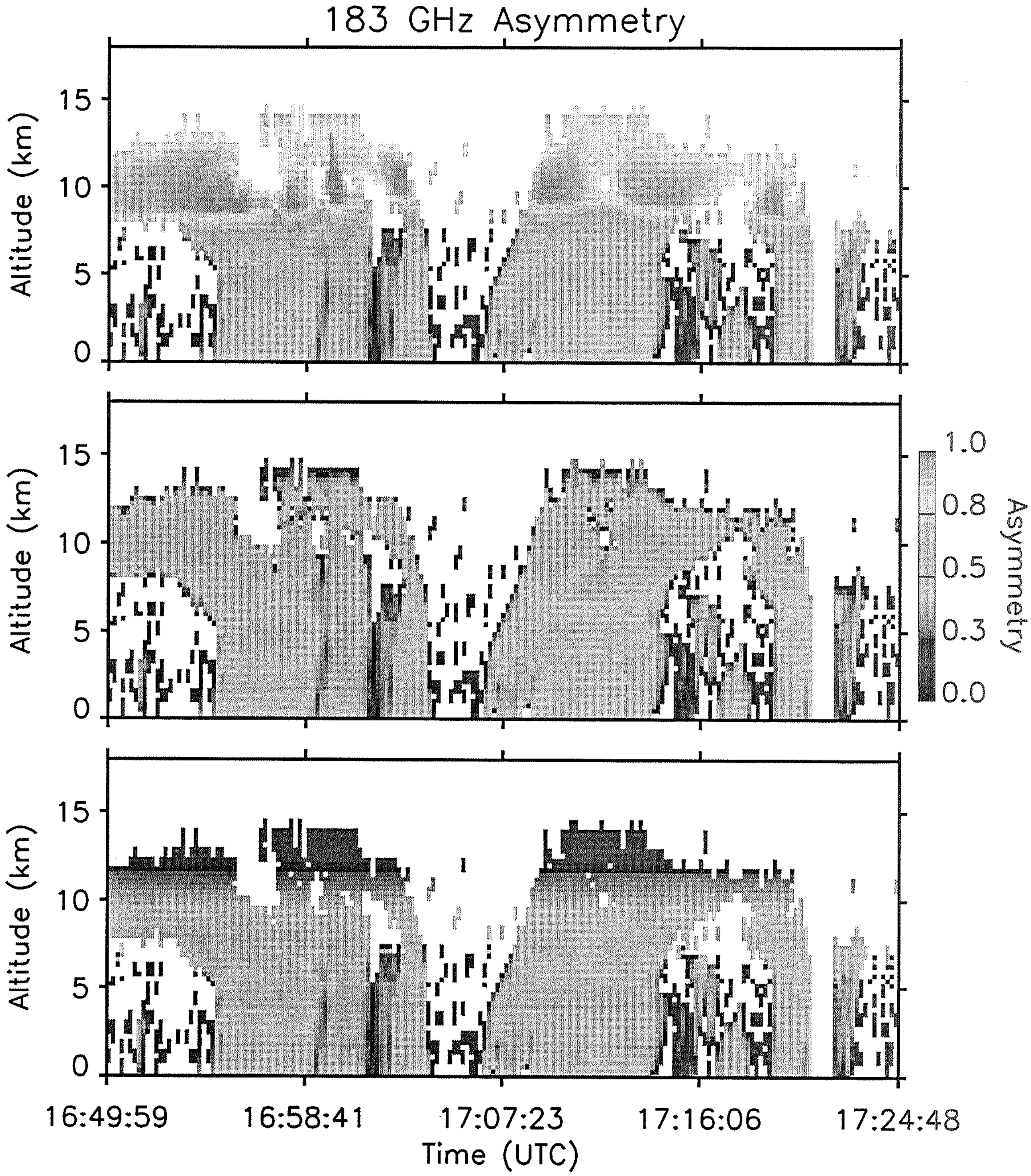

Figure 5: Bulk asymmetry fields at 183±7 GHz for (a) fluffy spheres, (b) solid ice SS spheres, and (c) three-dimensional rosettes. Asymmetry factors are unitless.

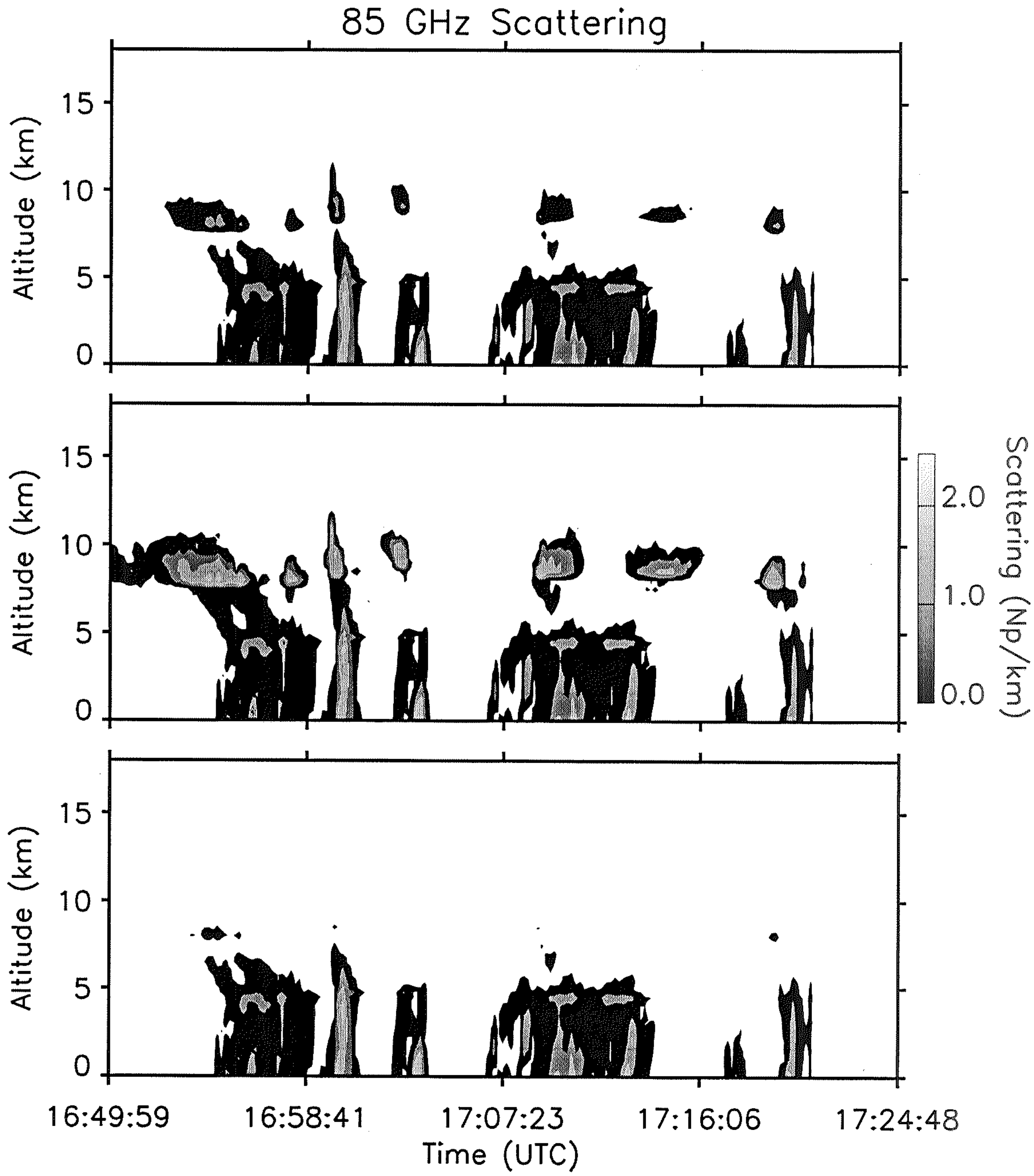

Figure 6: Bulk scattering fields at 85 GHz for (a) fluffy spheres, (b) solid ice SS spheres, and (c) three-dimensional rosettes. Shading thresholds are at 0.1, 0.5, 1.0, 2.0, 3.0, and 4.0 nepers/km.

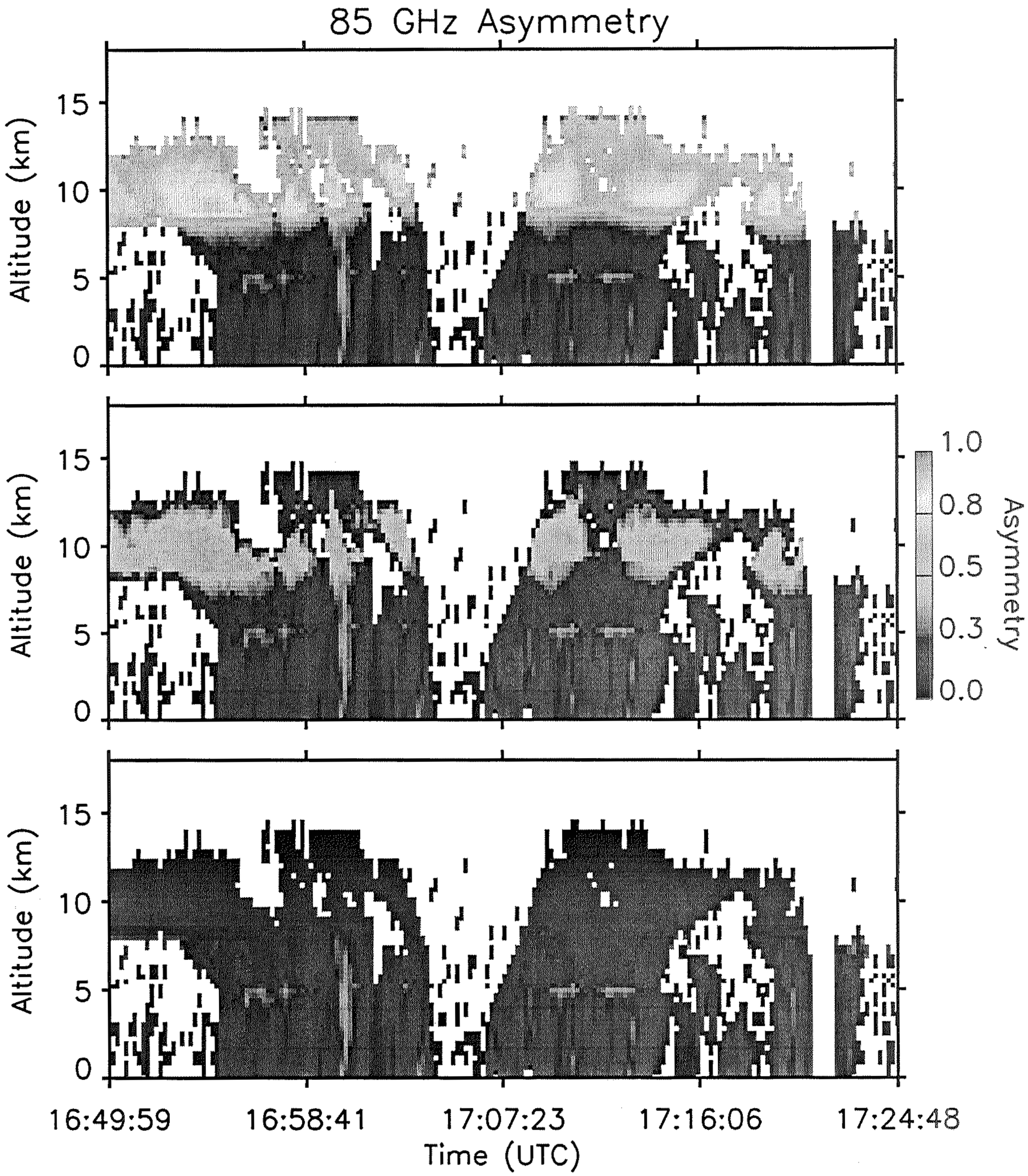

Figure 7: Bulk asymmetry fields at 85 GHz for (a) fluffy spheres, (b) solid ice SS spheres, and (c) three-dimensional rosettes. Asymmetry factors are unitless.

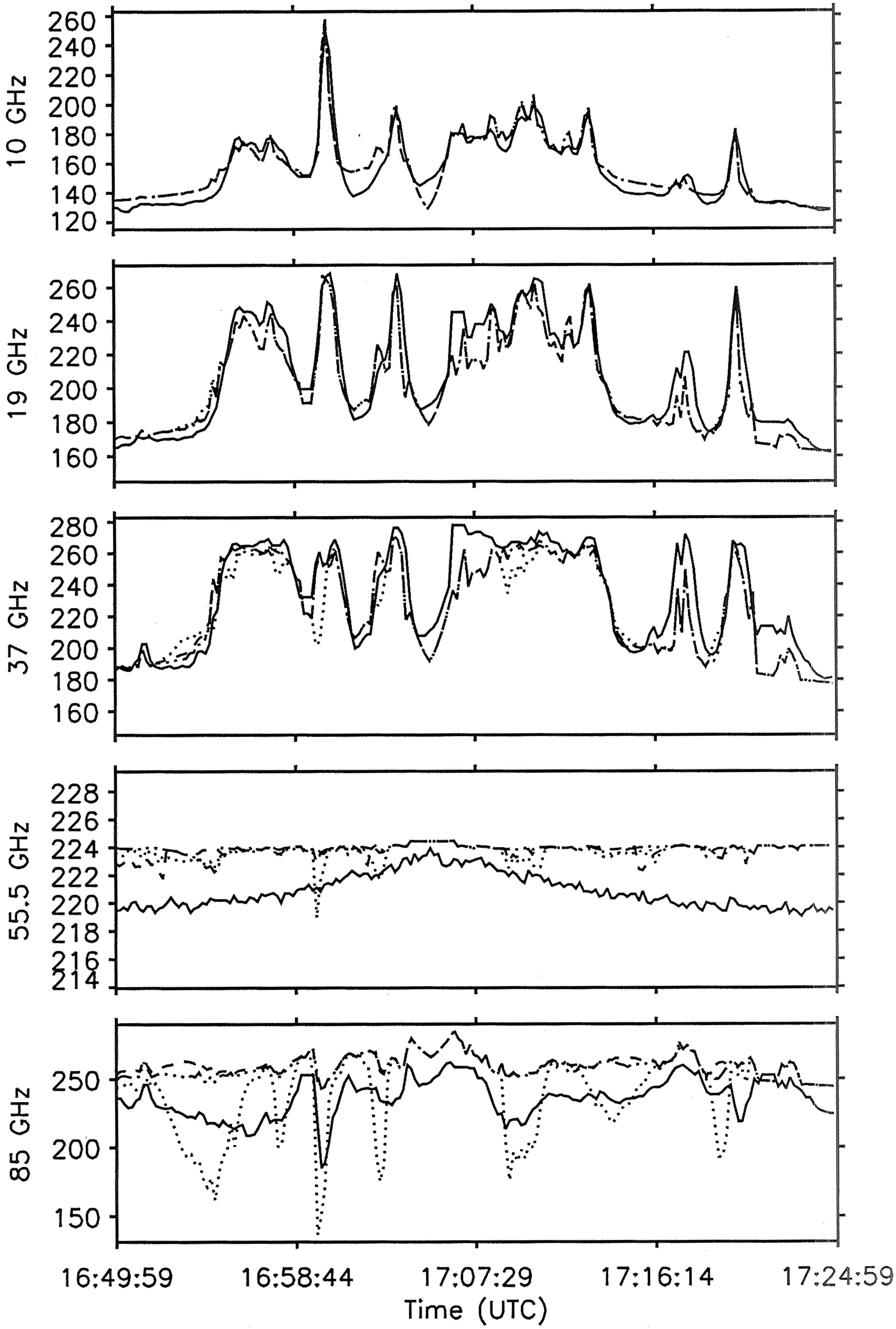
10 GHz
260
240
220
200
180
160
140
120
19 GHz
260
240
220
200
180
160
37 GHz
280
260
240
220
200
180
160
55.5 GHz
228
226
224
222
220
218
216
214
85 GHz
250
200
150
16:49:59
16:58:44
17:07:29
17:16:14
17:24:59
Time (UTC)

812

813

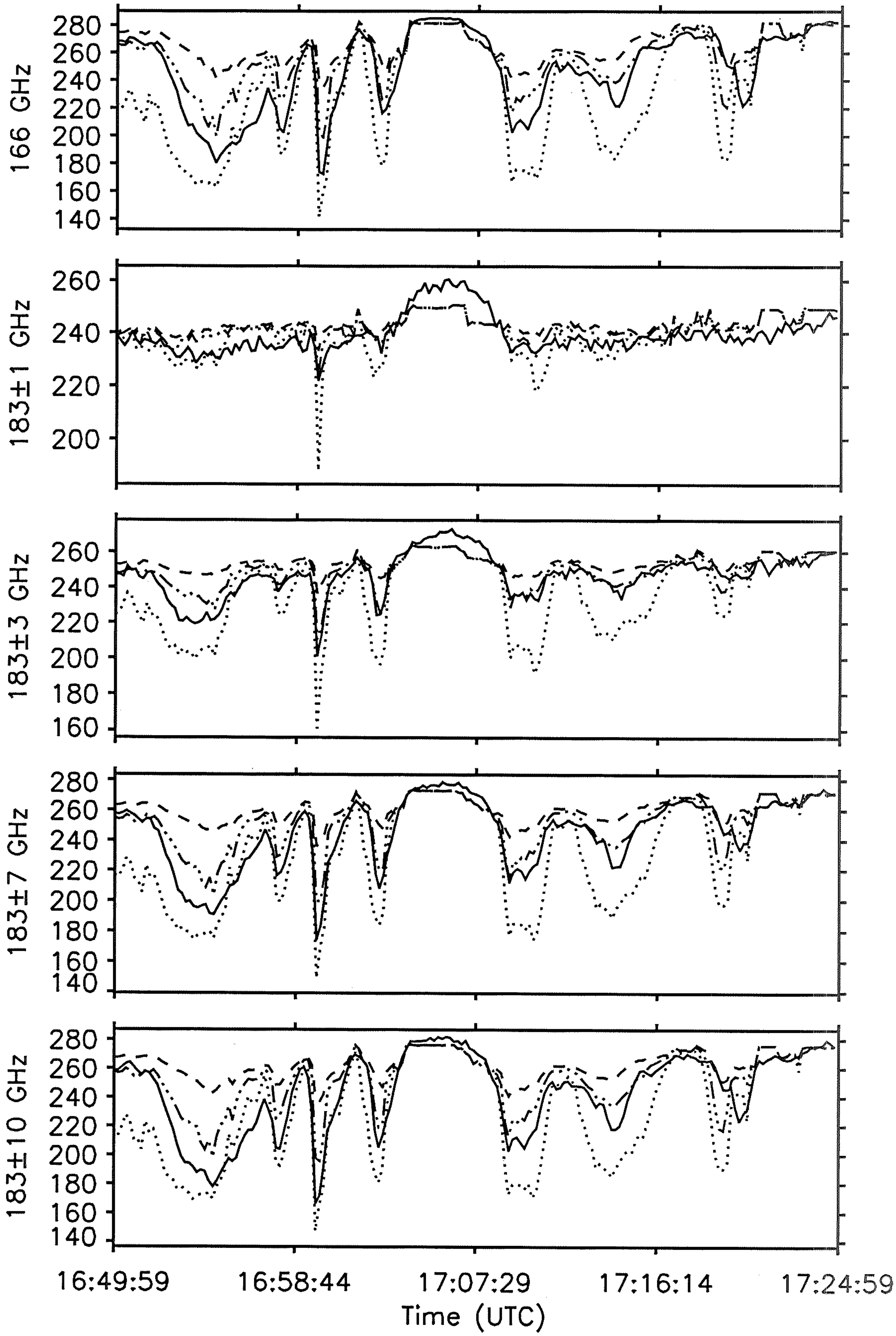
280
260
240
220
200
180
160
140
166 GHz
260
240
220
200
183±1 GHz
260
240
220
200
180
160
183±3 GHz
280
260
240
220
200
180
160
140
183±7 GHz
280
260
240
220
200
180
160
140
183±10 GHz
16:49:59
16:58:44
17:07:29
17:16:14
17:24:59
Time (UTC)

Figure 6: Brightness temperature values for 10, 19, 37, 55.5, and 85 GHz in Kelvin for the observations (solid line), SS parameterization (dotted line), Fluffy parameterization (dashed line), and Rosette parameterization (dash-dotted line).

Figure 7: Same as Figure 6 except for 166, 183.3±1, ±3, ±7, ±10 GHz.